Acta Mechanica 69. 219–241 (1987)

ACTA MECHANICA
© by Springer-Verlag 1987

A Bimodal Plasticity Theory of Fibrous Composite Materials*

By

G. J. Dvorak and **Y. A. Bahei-El-Din**, Troy, New York

With 9 Figures

(Received December 1, 1986, revised June 17, 1987)

Summary

It is shown that elastic-plastic response of metal matrix composites reinforced by aligned continuous fibers can be described in terms of two distinct modes. In the matrix-dominated mode, the composite deforms primarily by plastic slip in the matrix, on planes which are parallel to the fiber axis. In the fiber-dominated mode, both phases deform together in the elastic and plastic range. Constitutive equations are derived for the matrix-dominated mode of deformation in composites with elastic-perfectly plastic matrices. Response in the fiber-dominated mode is approximated by the self-consistent and Voigt models The two deformation modes give different branches of the overall yield surface which identify the state of stress that activates a particular mode, and indicate the conditions for mode transition in a given composite system. The matrix-dominated mode is found to exist in systems reinforced by fibers of large longitudinal shear stiffness, such as boron or silicon carbide. Systems reinforced by more compliant fibers, such as graphite, appear to deform exclusively in the fiber-dominated mode. The results show good agreement with experimental data, and with predictions obtained from a more accurate material model. They also help to reconcile several different plasticity theories of fibrous composites, and suggest limits of their validity

1. Introduction

This paper explores certain new aspects of plastic deformation of metal matrix composite materials reinforced by aligned continuous fibers, which were revealed, in part, in the course of a recent experimental program conducted in cooperation with Professor Phillips in his laboratory at Yale University.

To introduce the subject, imagine that an unreinforced elastic-plastic layer is subjected to incremental loading by macroscopically uniform states of plane stress. At each point of the loading path there is a certain macroscopically uniform plastic strain rate field which may be related, e.g., through Tresca or Mises yield conditions, to a hypothetical family of slip planes and directions on which the

* Prepared for the Symposium on Plasticity: Foundations and Future Directions. In Memory of Aris Phillips. January 28–30, 1987. University of Florida, Gainesville, U.S A

overall field is resolved into simple shear deformations. Now, if the layer is reinforced by aligned, elastic fibers, and subjected to the same incremental loading history, plastic slip may still take place on those planes which are parallel to the fiber axis, but not necessarily on planes which intersect the fibers. Slip on the intersecting planes may be impeded to a certain extent, depending on the fiber properties and the state of stress. For example, fibers with large shear stiffness, such as boron, silicon carbide. or alumina (FP), may render all off-axis planes inactive in a wide range of stress states; whereas fibers which are more compliant in shear, such as graphite, may only have a limited effect.

These considerations suggest that elastic-plastic response of the fibrous ply may be analyzed in terms of two distinct deformation modes. In the case of stiff elastic fibers, macroscopic plastic straining will be preferred in certain directions, through local deformation of the matrix interlayers which are, in actual composite systems, only 10–100μ thick. Under such circumstances one expects that simple shear will be the dominant mode of local plastic deformation of the matrix, and that the fiber will not participate in this mode. Therefore, the composite ply may be regarded as an elastic-plastic continuum with slip planes parallel to the fiber axis. Apart from this restriction, the ply deforms plastically in the same way as the matrix, and therefore, this type of deformation will be referred to as the matrix-dominated mode.

In systems reinforced by more compliant elastic fibers, and under overall stresses which do not favor the matrix mode, both phases must deform together in the elastic and plastic range. The fiber often has a significant influence on the overall response, hence this case will be referred to as the fiber-dominated mode. No particular deformation mechanism is suggested, the mode must be treated as a general case of plastic deformation of heterogeneous medium.

Of course, a theory which can be applied to the general case should be able to predict both modes. It will be shown in the sequel that this is true for some theories, but not for others. In fact, certain approximate procedures appear to be adequate for the fiber-dominated mode, but not for the matrix-dominated mode. Therefore, it is desirable to have a plasticity theory which describes overall response in the matrix mode, and which indicates the conditions responsible for mode transition.

This paper considers elastic-plastic response of composite plies which may deform in either mode, depending on material properties and the state of stress. The matrix-dominated mode is analyzed first. This is followed by a brief description of the self-consistent and Voigt approximations which appear to represent certain aspects of ply behavior in the fiber-dominated mode. Each mode gives certain branches of the overall yield surface which is then found as their internal envelope. In each material system the overall yield surface identifies the stress states which can activate a particular deformation mode. The results are compared with experimental data, and discussed in terms of their connections with other theories.

2. Matrix Dominated Plastic Deformation

2.1 Yield Condition

Consider a thin layer of a fibrous composite under macroscopically uniform state of plane stress. The fibers are aligned in the direction of the Cartesian coordinate x_1, the x_1x_2-plane coincides with the midplane of the layer. Overall elastic properties of the layer are known in terms of elastic constants and volume fractions of the phases. In this section we consider only the matrix dominated mode of plastic deformation in the thin interlayers of matrix which seperate the stiff, aligned fibers. To model this deformation mode, we assume that the interlayers may deform plastically only by simple shear on planes parallel to the fiber axis. Although the matrix is a polycrystal, the assumption implies that the kinematics of plastic deformation of the composite is somewhat similar to that of a single crystal. Therefore, in the analysis that follows we regard the fibrous aggregate as an anisotropic continuum with slip planes parallel to the fiber axis x_1, and use several results from single crystal plasticity to obtain its overall response. Figure 1 shows the geometry of the two conjugate slip systems $k = 1, 2$, that may become active under a macroscopic state of plane stress in the x_1x_2-plane, $\boldsymbol{n}_k$ denotes the normal to the slip plane, and $\boldsymbol{s}_k$ the slip direction.

Let

$$\beta = \beta_1 = \pi - \beta_2, \qquad \theta = \theta_1 = \theta_2. \tag{1}$$

Then,

$$\begin{aligned} \boldsymbol{n}_1 &= [0, \cos\beta, -\sin\beta] \\ \boldsymbol{s}_1 &= [\cos\theta, \sin\beta\sin\theta, \cos\beta\sin\theta] \end{aligned} \tag{2}$$

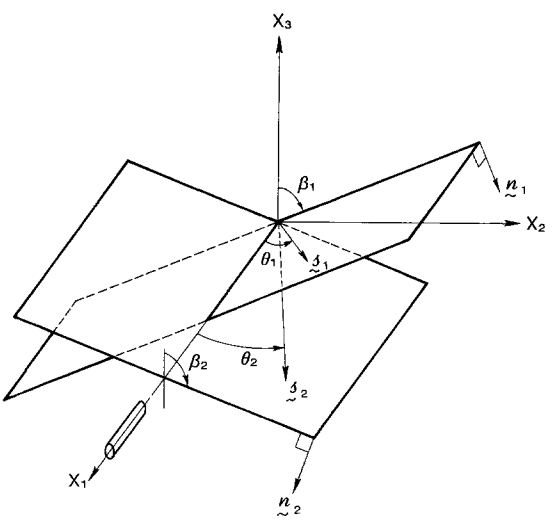

Fig. 1. Geometry of conjugate slip systems of the matrix-dominated deformation mode

$$\boldsymbol{n}_2 = [0, -\cos\beta, -\sin\beta]$$
$$\boldsymbol{s}_2 = [\cos\theta, \sin\beta\sin\theta, -\cos\beta\sin\theta]. \tag{3}$$

The resolved shear stress on the plane $\boldsymbol{n}_k$ in the direction $\boldsymbol{s}_k$ is

$$\tau_{ns}^{(k)} = n_i^{(k)} \sigma_{ij} s_j^{(k)}, \tag{4}$$

and for the plane stress case considered:

$$\tau_{ns}^{(1)} = \frac{1}{2}\sin 2\beta \sin\theta\, \sigma_{22} + \cos\beta\cos\theta\, \sigma_{21} \tag{5}$$

$$\tau_{ns}^{(2)} = -\tau_{ns}^{(1)}. \tag{6}$$

The matrix-dominated mode of plastic deformation of the fibrous composite medium can be quite complex on the microscale. For example, slip in the longitudinal direction x_1 takes place on surfaces parallel to x_1. In contrast, slip in the transverse direction, with $\boldsymbol{s}$ perpendicular to x_1, may involve interaction of slip planes with individual fibers, except perhaps in composite plies reinforced by monolayers of fiber. Accordingly, one would anticipate the macroscopic flow stress τ_0 to depend on the direction of $\boldsymbol{s}$. However, both micromechanical modeling of plastic flow in the fibrous medium [1], [2], and the experimental results presented in the sequel indicate that the directional dependence of τ_0 is negligible.

Therefore, the yield condition for each slip plane k can be written as

$$f^{(k)}(\tau) \equiv (\max \tau_{ns}^{(k)})^2 - \tau_0^2 = 0, \tag{7}$$

where $\tau_0 > 0$ is the matrix or ply yield stress in simple shear. To find a specific form of (7) in terms of the applied stress, it is necessary to evaluate the maxima of $\tau_{ns}^{(k)}$ (β, θ).

For $k = 1$, from (5):

$$\begin{aligned} \partial\tau_{ns}^{(1)}/\partial\beta &= \sigma_{22}(\cos 2\beta \sin\theta - q\sin\beta\cos\theta) = 0 \\ \partial\tau_{ns}^{(1)}/\partial\theta &= \sigma_{22}\left(\frac{1}{2}\sin 2\beta\cos\theta - q\cos\beta\sin\theta\right) = 0, \end{aligned} \tag{8}$$

where

$$q = \sigma_{21}/\sigma_{22}, \qquad \text{for} \quad \sigma_{22} \neq 0. \tag{9}$$

It can be verified that equations (8) give maxima of $\tau_{ns}^{(k)}$, and that their solution is:

For $|q| \leqslant 1$:

$$\begin{aligned} \sin\beta_1 &= \left[\frac{1}{2}(1-q^2)\right]^{1/2} = q\tan\theta_1 \\ \cos\beta_1 &= \left[\frac{1}{2}(1+q^2)\right]^{1/2} \\ \sin\theta_1 &= [(1-q^2)/(1+q^2)]^{1/2} = \tan\beta_1 \\ \cos\theta_1 &= [2q^2/(1+q^2)]^{1/2}. \\ 0 \leqslant \beta_1 &\leqslant \pi/4: \quad 0 \leqslant \theta_1 \leqslant 2\pi \end{aligned} \tag{10}$$

and, for $|q| \geqslant 1$:

$$\begin{aligned} &\beta_1 = 0 \\ &\theta_1 = 0 \text{ for } \sigma_{21} = \tau_0, 0 < \sigma_{22} < \tau_0 \\ &\theta_1 = \pi \text{ for } \sigma_{21} = -\tau_0 \\ &\theta_1 = 2\pi \text{ for } \sigma_{21} = \tau_0, 0 > \sigma_{22} > -\tau_0. \end{aligned} \tag{11}$$

For the conjugate slip system $k = 2$, one can write from equations (1) and (6), in analogy with (10) and (11):

For $|q| \leqslant 1$:

$$\begin{aligned} &\sin\beta_2 = \sin\beta_1, \quad \cos\beta_2 = -\cos\beta_1 \\ &\sin\theta_2 = \sin\theta_1, \quad \cos\theta_2 = \cos\theta_1 \\ &\pi \geqslant \beta_2 \geqslant 3\pi/4, \qquad 0 \leqslant \theta_2 \leqslant 2\pi \end{aligned} \tag{12}$$

and, for $|q| \geqslant 1$:

$$\beta_2 = 0, \qquad \theta_2 = \theta_1. \tag{13}$$

The maxima of τ_{ns} can now be found for the two parts of the solution of equations (8). Substitute (10) or (12) into (5) or (6), respectively, to obtain:

$$\max \tau_{ns}^{(1)} = -\max \tau_{ns}^{(2)} = \frac{1}{2}(1 - q^2)\sigma_{22} + q\sigma_{21}, \quad \text{for } |q| \leqslant 1 \tag{14}$$

and, from (13) and (5) or (6):

$$\max \tau_{ns}^{(1)} = -\max \tau_{ns}^{(2)} = \sigma_{21}, \quad \text{for } |q| \geqslant 1. \tag{15}$$

The direction of $\max \overset{(k)}{\tau}_{ns}$ coincides with that of $\boldsymbol{s}_k$ in equations (2) or (3), taken for values of β_k, θ_k ($k = 1, 2$), given by (10) to (13). The sign of $\max \tau_{ns}^{(k)}$ refers to the direction of the shear stress vector in the coordinates of Fig. 1. Note that the absolute value of the terms in equation (14) does not depend on the respective signs of σ_{22} and σ_{21}.

Now, the maxima of $\tau_{ns}^{(k)}$, given by equations (14) and (15), may be substituted in the yield condition (7). As expected, both slip systems $k = 1, 2$ start to yield at the same macroscopic stress level, hence a single overall yield surface $f(\boldsymbol{\sigma})$ exists in the stress space σ_{ij}. However, because the $\max \tau_{ns}^{(k)}$ are given by the two different forms (14) and (15), the overall yield surface has two branches.

The first branch, for $|q| \leqslant 1$, will be denoted by $f_a(\boldsymbol{\sigma})$; it is given by

$$f_a(\boldsymbol{\sigma}) \equiv \frac{1}{4}\sigma_{22}^2(1 + q^2)^2 - \tau_0^2 = 0. \tag{16}$$

If q is eliminated from equation (16), then one obtains

$$f_a(\boldsymbol{\sigma}) \equiv \left(\frac{\sigma_{21}}{\tau_0}\right)^2 + \left(\frac{\sigma_{22}}{\tau_0} \mp 1\right)^2 - 1 = 0. \tag{17}$$

The second branch of the overall yield surface , for $|q| \geqslant 1$, will be denoted

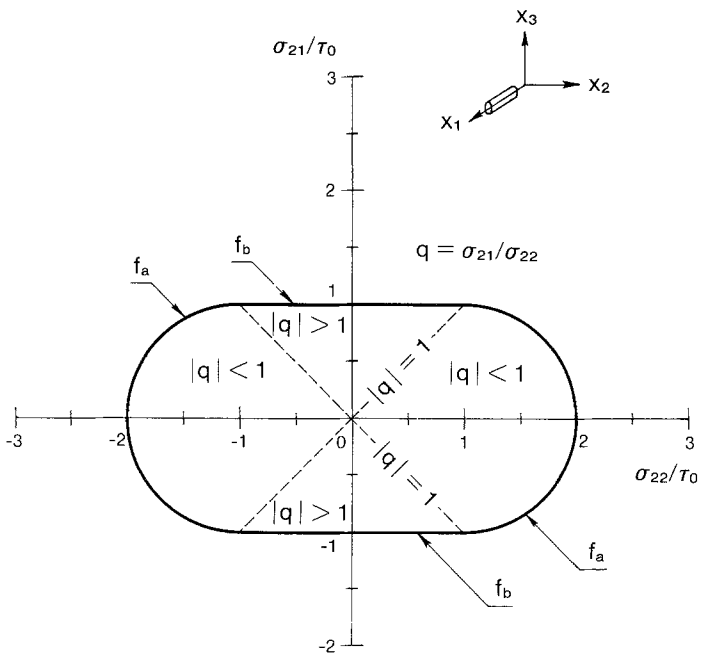

Fig. 2 Transverse cross section of the initial yield surface of the matrix-dominated mode

by $f_b(\boldsymbol{\sigma})$. It is obtained from equations (7) and (15) as:

$$f_b(\boldsymbol{\sigma}) \equiv \sigma_{21}^2 - \tau_0^2 = 0. \tag{18}$$

Note that at $|q| = 1$ the two branches coincide.

The cross section of the overall yield surface is shown in Fig. 2, the complete surface is an infinite cylinder with axis σ_{11}. Figure 3 indicates the magnitudes of the angles β and θ for the slip system $k = 1$ at different points of the two branches of the yield surface. Note that the magnitudes of β and θ are indicated by the distance, measured along the normal to the yield surface. between the yield surface itself and the β and θ curves. It is now apparent that on the branch $f_a(\boldsymbol{\sigma})$, which is a function of q, there is $\sigma_{22} \neq 0$. as demanded by the definition of q in equation (9).

2.2 Stress-Strain Relations

The rate of deformation is given by

$$d\boldsymbol{\varepsilon} = d\boldsymbol{\varepsilon}^e + d\boldsymbol{\varepsilon}^p. \tag{19}$$

The elastic part is

$$d\boldsymbol{\varepsilon}^e = \boldsymbol{M}_e\, d\boldsymbol{\sigma} \tag{20}$$

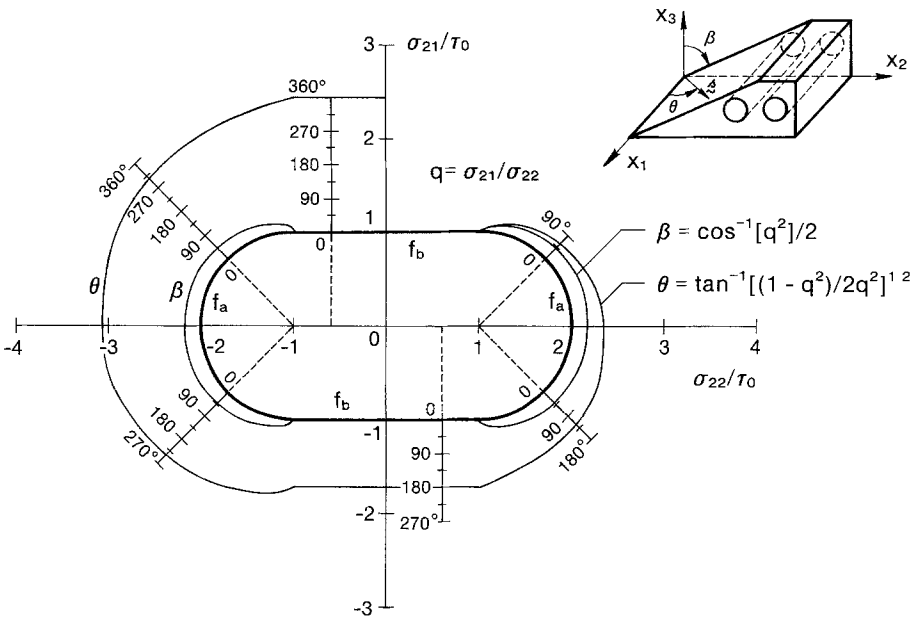

Fig. 3. Values of the angles β and θ at initial yielding, as functions of the applied stress ratio $q = \sigma_{21}/\sigma_{22}$

where $\boldsymbol{M}_e$ is the elastic compliance matrix. For the plane stress case this becomes:

$$\begin{aligned} d\,\varepsilon_{11}^e &= (1/E_A)\,d\,\sigma_{11} - (\nu_A/E_A)\,d\,\sigma_{22} \\ d\,\varepsilon_{22}^e &= -(\nu_A/E_A)\,d\,\sigma_{11} + (1/E_T)\,d\,\sigma_{22} \\ d\,\varepsilon_{33}^e &= -(\nu_A/E_A)\,d\,\sigma_{11} - (\nu_T/E_T)\,d\,\sigma_{22} \\ 2\,d\,\varepsilon_{21}^e &= (1/G_A)\,d\,\sigma_{21}, \end{aligned} \tag{21}$$

where E_A, G_A, ν_A are overall elastic constants of the composite for axial extension and longitudinal shear, and E_T, ν_T the Young's modulus and Poisson's ratio in the transverse plane.

In evaluation of the plastic part of the strain rate, we assume that the matrix does not harden, and that constraint hardening caused by phase interactions on the slip planes can be neglected. This implies that τ_0 in equations (7), (16), and (18) remains constant during plastic deformation. Also, we assume that on each slip plane the plastic strain rate vector is normal to the local yield surface at the current loading point.

To examine the consequences of normality on the active slip plane k, we introduce local stress coordinates τ_1, τ_2 in this plane. In the slip planes shown in Fig. 1, τ_1 is parallel to x_1, and τ_2 is perpendicular to x_1. From equation (5), for $\theta = 0$, and $\theta = \pi/2$, respectively:

$$\tau_1 = \sigma_{21}\cos\beta, \quad \tau_2 = \sigma_{22}\sin\beta\cos\beta. \tag{22}$$

In these coordinates the yield condition (7) is a circle

$$f^{(k)}(\boldsymbol{\tau}) \equiv \tau_1^2 + \tau_2^2 - \tau_0^2 = 0 \tag{23}$$

on each plane k.

It now follows from equation (22) that in the overall stress coordinates the yield condition (23) is

$$f^{(k)}(\boldsymbol{\sigma}) = (\sigma_{21}^2 + \sigma_{22}^2 \sin^2\beta)\cos^2\beta. \tag{24}$$

It can be verified that for $|q| \leqslant 1$ equation (24) gives the $f_a(\boldsymbol{\sigma})$ branch (16) of the overall yield surface. providing that β is taken from equations (10) and (12). Similarly, for $|q| \geqslant 1$, and β taken from equations (11) and (13), one recovers from equation (24) the $f_b(\boldsymbol{\sigma})$ branch given by equation (18). Therefore, the overall yield surface (16) to (18) is a projection of the local surface (23) from its original $\tau_1\tau_2$-plane into the overall $\sigma_{22}\sigma_{21}$-plane. Since the local surface is a circle, the current loading vector coincides with the direction of its outside normal at the loading point.

The normality condition for the local plastic strain rate then suggests that on each active slip plane k:

$$d\gamma_{ns}^p = d\lambda \max \tau_{ns}^{(k)}. \tag{25}$$

The overall plastic strain rate is obtained as a sum of all local contributions in the form

$$d\varepsilon_{ij}^p = \sum_k (n_i s_j + s_i n_j)\, d\gamma_{ns}^p/2, \tag{26}$$

where the summation is taken over all active slip planes. The components of $\boldsymbol{s}_k$ and $\boldsymbol{n}_k$ for $k = 1, 2$ are given by equations (2) and (3) and by the extremum conditions (10) to (13). Specific results are:

For $|q| \leqslant 1$:

$$\begin{aligned} d\varepsilon_{11}^p &= 0 \\ d\varepsilon_{22}^p &= \frac{1}{2} d\lambda (1 - q^4)\sigma_{22} \\ d\varepsilon_{33}^p &= -\frac{1}{2} d\lambda (1 - q^4)\sigma_{22} = -d\varepsilon_{22}^p \\ 2\, d\varepsilon_{32}^p &= 2\, d\varepsilon_{31}^p = 0 \\ 2\, d\varepsilon_{21}^p &= d\lambda (1 + q^2)\sigma_{21}. \end{aligned} \tag{27}$$

For $|q| \geqslant 1$:

$$\begin{aligned} d\varepsilon_{ij}^p &= 0 \quad \text{for} \quad ij \neq 21 \\ 2\, d\varepsilon_{21}^p &= 2\, d\lambda\, \sigma_{21}. \end{aligned} \tag{28}$$

Note that (27) implies that the composite ply is plastically incompressible in the matrix-dominated deformation mode.

It is possible to show that normality and consistency on each active slip plane guarantees normality and consistency on the macroscale. In particular,

from the local strain increment used in equation (26), with (1) to (3):

$$d\varepsilon_{22}^{p} = 4\sin\beta\cos\beta\sin\theta\, d\gamma_{ns}^{p}/2 \tag{29.1}$$

$$2\,d\varepsilon_{21}^{p} = 4\cos\beta\cos\theta\, d\gamma_{ns}^{p}/2, \tag{29.2}$$

where β and θ are given by equations (10) to (13).

Therefore, for $|q| \leqslant 1$ one obtains:

$$\frac{d\varepsilon_{22}^{p}}{2\,d\varepsilon_{21}^{p}} = \frac{1-q^2}{2q} \tag{30}$$

and for $|q| \geqslant 1$; using (5) and (11)

$$d\varepsilon_{22}^{p} = 0, \quad 2\,d\varepsilon_{21}^{p} = 2\,d\gamma_{ns}^{p} = 2\,d\lambda\,\sigma_{21}. \tag{31}$$

Note that these expressions are consistent with (29.2) when $|q| = 1$ and $\beta \to 0$, $\theta \to 0$, and that they imply the existence of two conjugate slip systems even for $|q| \geqslant 1$.

Equations (30) and (31) can also be derived from the normality condition for the plastic strain vector on the macroscale.

For $|q| \leqslant 1$, from equation (16):

$$\frac{d\varepsilon_{22}^{p}}{2\,d\varepsilon_{21}^{p}} = \frac{d\lambda\,\partial f_a(\boldsymbol{\sigma})/\partial\sigma_{22}}{d\lambda\,\partial f_a(\boldsymbol{\sigma})/\partial\sigma_{21}} = \frac{1-q^2}{2q}, \tag{32}$$

and for $|q| \geqslant 1$, from equation (18):

$$\begin{aligned} d\varepsilon_{22}^{p} &= d\lambda\,\partial f_b(\boldsymbol{\sigma})/\partial\sigma_{22} = 0, \\ 2\,d\varepsilon_{21}^{p} &= d\lambda\,\partial f_b(\boldsymbol{\sigma})/\partial\sigma_{21} = 2\,d\lambda\,\sigma_{21}. \end{aligned} \tag{33}$$

Next, the equation of consistency for the local yield function (7) is:

$$df^{(k)}(\tau) = 2\max\tau_{ns}^{(k)}\, d\tau_{ns}^{(k)} = 0. \tag{34}$$

Using equations (5), (6), and (9) to (13) one obtains:

$$\frac{d\sigma_{22}}{d\sigma_{21}} = -\frac{2q}{1-q^2}, \qquad \text{for } |q| \leqslant 1 \tag{35}$$

and

$$d\sigma_{21} = 0, \qquad \text{for } |q| \geqslant 1. \tag{36}$$

In a similar way, the equations of consistency for the macroscopic yield functions $f_a(\boldsymbol{\sigma})$ in equation (16) and $f_b(\boldsymbol{\sigma})$ in (18) lead to:

$$\frac{d\sigma_{22}}{d\sigma_{21}} = -\frac{2q}{1-q^2} = \frac{-2\,d\varepsilon_{21}^{p}}{d\varepsilon_{22}^{p}}, \quad \text{for } |q| \leqslant 1 \tag{37}$$

and

$$d\sigma_{21} = 0, \qquad \text{for } |q| \geqslant 1. \tag{38}$$

It is often advantageous to write the macroscopic stress-strain relations in terms of overall instantaneous stiffness rather than compliance. For $|q| \leqslant 1$,

equation (37) suggests that

$$d\sigma_{21} = -\rho\, d\sigma_{22}, \quad \text{where } \rho = \frac{(1-q^2)}{2q}. \tag{39}$$

Then, equation (19) can be written in terms of (21) and (27) as

$$d\varepsilon_{11} = (1/E_A)\, d\sigma_{11} - (\nu_A/E_A)\, d\sigma_{22} \tag{40.1}$$

$$d\varepsilon_{22} = -(\nu_A/E_A)\, d\sigma_{11} + (1/E_T)\, d\sigma_{22} + 2\rho\, d\varepsilon_{21}^{p} \tag{40.2}$$

$$d\varepsilon_{33} = -(\nu_A/E_A)\, d\sigma_{11} - (\nu_T/E_T)\, d\sigma_{22} - 2\rho\, d\varepsilon_{21}^{p} \tag{40.3}$$

$$2\, d\varepsilon_{21} = (1/G_A)\, d\sigma_{21} + 2\, d\varepsilon_{21}^{p}. \tag{40.4}$$

From equations (39), (40.1), (40.2), and (40.4) one obtains the overall instantaneous stress increments caused by applied strain increments:

$$\begin{aligned}
d\sigma_{11} &= \frac{1}{C_2}[C_4\, d\varepsilon_{11} + C_3\nu_A\, d\varepsilon_{22} - 2C_3\rho\nu_A\, d\varepsilon_{21}] \\
d\sigma_{22} &= \frac{1}{C_1}[\nu_A\, d\varepsilon_{11} + d\varepsilon_{22} - 2\rho\, d\varepsilon_{21}] \\
d\sigma_{33} &= d\sigma_{32} = d\sigma_{31} = 0 \\
d\sigma_{21} &= -\rho\, d\sigma_{22},
\end{aligned} \tag{41}$$

where:

$$\begin{aligned}
C_1 &= \left[\frac{1}{E_T} - \frac{\nu_A^2}{E_A} + \frac{\rho^2}{G_A}\right] \\
C_2 &= \left[\frac{1}{E_T} - \frac{\nu_A^2}{E_A}\right] \\
C_3 &= [1 - \rho^2/(G_A C_1)] \\
C_4 &= \left[\frac{E_A}{E_T} - \frac{\nu_A^2\rho^2}{G_A C_1}\right].
\end{aligned}$$

For $|q| \geqslant 1$ one can derive similar results from equations (19), (21), (28), and (38):

$$\begin{aligned}
d\varepsilon_{11} &= (1/E_A)\, d\sigma_{11} - (\nu_A/E_A)\, d\sigma_{22} \\
d\varepsilon_{22} &= -(\nu_A/E_A)\, d\sigma_{11} - (\nu_A/E_A)\, d\sigma_{22} \\
d\varepsilon_{33} &= -(\nu_A/E_A)\, d\sigma_{11} - (\nu_T/E_T)\, d\sigma_{22} \\
2\, d\varepsilon_{21} &= 2\, d\varepsilon_{21}^{p} \\
d\sigma_{11} &= \frac{1}{C_2}[(E_A/E_T)\, d\varepsilon_{11} + \nu_A\, d\varepsilon_{22}] \\
d\sigma_{22} &= \frac{1}{C_2}[\nu_A\, d\varepsilon_{11} + d\varepsilon_{22}] \\
d\sigma_{21} &= d\sigma_{33} = d\sigma_{32} = d\sigma_{31} = 0.
\end{aligned} \tag{42}$$

3. Fiber Dominated Plastic Deformation

3.1 Local Fields

Consider again the thin layer of a fibrous composite under macroscopically uniform state of plane stress, described in Section 2.1. The elastic properties of the layer remain unchanged. However, plastic deformation in the matrix is now regarded in terms of the fiber-dominated mode, in which the applied stress may activate slip on many planes that intersect the fiber axis. Matrix-dominated plastic deformation of the ply is suppressed to allow examination of the fiber-dominated mode in the entire plane stress space. Therefore, simultaneous deformation of both phases must be considered in the plastic range.

Accurate micromechanical modeling of such plastic deformation processes is rather difficult; a comprehensive treatment appears in references [1] and [2]. Our present scope is more limited. We wish to analyze the fiber-dominated mode in an approximate manner which would allow us to identify the boundary between the two deformation modes in the overall stress space, and which would also permit evaluation of plastic strains of the fiber-dominated mode in material systems where it is not particularly prominent. This purpose is served by an approximation in which the overall response of the composite aggregate is derived from certain averaged responses of the phases.

In particular, we adopt and review briefly, the approach and notation developed by Hill [3]. The volume averages of stress and strain increments in the phases are described by (6×1) column vectors $d\boldsymbol{\sigma}_r$, $d\boldsymbol{\varepsilon}_r$, $r = f, m$, and related to the applied overall uniform increments $d\boldsymbol{\sigma}$, $d\boldsymbol{\varepsilon}$ through certain (6×6) matrices, or concentration factors:

$$d\boldsymbol{\varepsilon}_f = \boldsymbol{A}_f d\boldsymbol{\varepsilon}, \qquad d\boldsymbol{\varepsilon}_m = \boldsymbol{A}_m d\boldsymbol{\varepsilon} \tag{43.1,2}$$

$$d\boldsymbol{\sigma}_f = \boldsymbol{B}_f d\boldsymbol{\sigma}, \qquad d\boldsymbol{\sigma}_m = \boldsymbol{B}_m d\boldsymbol{\sigma}. \tag{44.1,2}$$

The phase and volume averages are related by

$$c_f d\boldsymbol{\varepsilon}_f + c_m d\boldsymbol{\varepsilon}_m = d\boldsymbol{\varepsilon}; \quad c_f d\boldsymbol{\sigma}_f + c_m d\boldsymbol{\sigma}_m = d\boldsymbol{\sigma}, \tag{45}$$

where $c_f + c_m = 1$ are phase volume fractions.

The local constitutive relations for the phase volume averages are assumed to be known in the form

$$d\boldsymbol{\varepsilon}_r = \boldsymbol{M}_r d\boldsymbol{\sigma}_r, \quad d\boldsymbol{\sigma}_r = \boldsymbol{L}_r d\boldsymbol{\varepsilon}_r, \quad (r = f, m) \tag{46}$$

where $\boldsymbol{M}_r$, $\boldsymbol{L}_r$ are instantaneous compliance and stiffness matrices of the phases. In an elastic phase the local properties are constant, hence equations (46) are exact. However, if the phase deforms plastically, its properties become stress-dependent. Then, equation (46) can be accepted only as an approximation which may become unsatisfactory if changes in the local fields are not sufficiently uniform.

In any event, the overall constitutive relations of the composite aggregate

can be written in the form

$$d\boldsymbol{\varepsilon} = \boldsymbol{M} d\boldsymbol{\sigma}, \quad d\boldsymbol{\sigma} = \boldsymbol{L} d\boldsymbol{\varepsilon} \tag{47}$$

and, if (46) is accepted, then it follows from equations (43) to (47) that

$$\boldsymbol{M} = c_f \boldsymbol{M}_f \boldsymbol{B}_f + c_m \boldsymbol{M}_m \boldsymbol{B}_m, \quad \boldsymbol{L} = c_f \boldsymbol{L}_f \boldsymbol{A}_f + c_m \boldsymbol{L}_m \boldsymbol{A}_m, \tag{48}$$

and that

$$c_f \boldsymbol{A}_f + c_m \boldsymbol{A}_m = c_f \boldsymbol{B}_f + c_m \boldsymbol{B}_m = \boldsymbol{I}, \tag{49}$$

where $\boldsymbol{I}$ is a (6×6) identity matrix.

Determination of overall properties is thus reduced to evaluation of one of the concentration factors which needs to be found for a selected model of the composite material.

For example, in the self-consistent model the concentration factors are obtained from solutions of inclusion problems in which each phase is embedded in an infinite, homogeneous composite medium under uniform overall strain or stress. In the elastic case, the concentration factors for a fibrous composite were derived, for example, by Walpole [4, Section 5]. Evaluation of their plastic counterparts is difficult [5] and possibly unreliable if equation (46) becomes inaccurate.

A particularly simple form of the concentration factors can be found if one adopts the Voigt assumption:

$$d\boldsymbol{\varepsilon}_f = d\boldsymbol{\varepsilon}_m = d\boldsymbol{\varepsilon} \tag{50}$$

which immediately gives

$$\boldsymbol{A}_f = \boldsymbol{A}_m = \boldsymbol{I} \tag{51}$$

and

$$\boldsymbol{L} = c_f \boldsymbol{L}_f + c_m \boldsymbol{L}_m. \tag{52}$$

Using equations (44), (46), and (47) one can write for each phase $r = f, m$.

$$d\boldsymbol{\sigma}_r = \boldsymbol{L}_r d\boldsymbol{\varepsilon}_r = \boldsymbol{B}_r \boldsymbol{L} d\boldsymbol{\varepsilon} \tag{53}$$

which, in combination with equation (50) gives:

$$\boldsymbol{B}_r = \boldsymbol{L}_r \boldsymbol{L}^{-1}, \tag{54}$$

where $\boldsymbol{L}$ follows from equation (52).

3.2 Yield Surfaces

The overall yield surface of a composite medium is a boundary of all stress points which can be reached from current state by purely elastic deformation. Suppose that the fibrous ply consists of an elastic fiber and an elastic-plastic matrix with a local yield surface given by

$$g_m(\boldsymbol{\sigma}_m - \boldsymbol{\alpha}_m) = 0, \tag{55}$$

where $\boldsymbol{\alpha}_m$ identifies the current position of the center. To each local stress vector

$(\boldsymbol{\sigma}_m - \boldsymbol{\alpha}_m)$ there corresponds the vector

$$(\boldsymbol{\sigma} - \boldsymbol{\alpha}) = \boldsymbol{B}_{me}^{-1}(\boldsymbol{\sigma}_m - \boldsymbol{\alpha}_m) \tag{56}$$

in the overall stress space; $\boldsymbol{B}_{me}$ is the elastic matrix stress concentration factor. Now, if the overall yield condition for onset of macroscopic plastic deformation is defined in terms of local stress averages, then it is the projection (56) of the surface g_m to the overall stress space $\boldsymbol{\sigma}$. This can be written as

$$g(\boldsymbol{\sigma} - \boldsymbol{\alpha}) = 0, \tag{57}$$

subject to (56).

Now, suppose that the composite aggregate is under current stress $\boldsymbol{\sigma}$ at yield, and subjected to a loading increment $d\boldsymbol{\sigma}$. The corresponding matrix stress increment follows from equation (44):

$$d\boldsymbol{\sigma}_m = \boldsymbol{B}_m d\boldsymbol{\sigma}, \tag{58}$$

where $\boldsymbol{B}_m$ is the stress concentration factor for elastic-plastic straining, given, for example, by equation (54). Differentiation of (56), and substitution from (58) gives, after rearrangement:

$$d\boldsymbol{\alpha} = (\boldsymbol{I} - \boldsymbol{B}_{me}^{-1}\boldsymbol{B}_m)\, d\boldsymbol{\sigma} + \boldsymbol{B}_{me}^{-1} d\boldsymbol{\alpha}_m, \tag{59}$$

which describes the incremental translation of g in (57), or overall strain hardening. The first term is caused by interaction between the phases and is referred to as constraint hardening. The second term represents the contribution, if it exists, of local or phase hardening to the overall response.

Of course, these results do not reflect the actual onset of plastic flow on the microscale, which depends on local stress gradients. Instead, they should be regarded as approximations of the overall yield surface for onset of macroscopic plastic deformation of the aggregate. In that regard, they are similar to the results obtained for matrix-dominated plastic deformation in Section 2.

As an example, we select g_m in the nonhardening Mises form:

$$g_m(\boldsymbol{\sigma}_m) \equiv \frac{1}{2}\boldsymbol{\sigma}_m^T \boldsymbol{Q}\boldsymbol{\sigma}_m - \tau_0^2 = 0, \tag{60}$$

where $\boldsymbol{\sigma}_m = [\sigma_{11}\sigma_{22}\sigma_{33}\sigma_{31}\sigma_{32}\sigma_{21}]_m^T$

$$\boldsymbol{Q} = \begin{bmatrix} \boldsymbol{q} & \vdots & \boldsymbol{O} \\ \cdots & \cdots & \cdots \\ \boldsymbol{O} & . & 2\boldsymbol{I}_3 \end{bmatrix}, \quad \boldsymbol{q} = \begin{bmatrix} 2/3 & -1/3 & -1/3 \\ & 2/3 & -1/3 \\ \text{sym.} & & 2/3 \end{bmatrix}$$

We recall that according to equation (59) $d\boldsymbol{\alpha} \neq \boldsymbol{0}$ even if $d\boldsymbol{\alpha}_m = \boldsymbol{0}$. Hence the transformation (56) of equation (60) gives the overall yield surface (57) in the form:

$$g(\boldsymbol{\sigma} - \boldsymbol{\alpha}) = \frac{1}{2}(\boldsymbol{\sigma} - \boldsymbol{\alpha})^T (\boldsymbol{B}_{me}^T \boldsymbol{Q}\boldsymbol{B}_{me})(\boldsymbol{\sigma} - \boldsymbol{\alpha}) - \tau_0^2 = 0, \tag{61}$$

with $\boldsymbol{\alpha} = \boldsymbol{0}$ for an initial yield surface of a stress-free composite.

3.3 Stress-Strain Relations

The connections between volume averages of local and overall stresses and strains can be utilized to estimate overall strains of the plastically deforming composite aggregate.

To illustrate the procedure, we use the Mises form (60) of g_m, and as in equations (32), or (33), write for the matrix plastic strain.

$$d\,\varepsilon_{ij}^{mp} = d\,\lambda\,\partial\,g_m/\partial\,\sigma_{ij}^{m}. \tag{62}$$

Since $d\lambda$ is not known, it is best to add the elastic strain to $d\,\varepsilon_{ij}^{mp}$, and find the stresses in terms of strains, as in equations (41) and (42). The inversion can be found in [6], and written as:

$$d\,\boldsymbol{\sigma}_m = (\boldsymbol{L}_{me} - G_m\,\boldsymbol{s}_m\,\boldsymbol{s}_m^T/\tau_0^2)\,d\,\boldsymbol{\varepsilon}_m, \tag{63}$$

where $\boldsymbol{L}_{me}$ is the elastic stiffness of the matrix material, $\boldsymbol{s}_m$ is matrix deviatoric stress vector, and G_m is the elastic shear modulus.

If the deviatoric stress $\boldsymbol{s}_m$ is found from a variant of equation (44.2):

$$\boldsymbol{s}_m = \hat{\boldsymbol{B}}_m\,\boldsymbol{\sigma}, \tag{64}$$

where $\hat{\boldsymbol{B}}_m$ is obtained from

$$\hat{\boldsymbol{B}}_m = \hat{\boldsymbol{Q}}\,\boldsymbol{B}_m, \quad \hat{\boldsymbol{Q}} = \begin{bmatrix} \boldsymbol{q} & \boldsymbol{0} \\ \cdots\cdots & \\ \boldsymbol{0} \;\vdots & \boldsymbol{I}_3 \end{bmatrix} \tag{65}$$

and $\boldsymbol{q}$ is given in (60), then, in equation (63), the instantaneous stiffness of the matrix material at current overall stress $\boldsymbol{\sigma}$ assumes the form:

$$\boldsymbol{L}_m = \boldsymbol{L}_{me} - \frac{G_m}{\tau_0^2}\,\hat{\boldsymbol{B}}_m\,\boldsymbol{\sigma}\,\boldsymbol{\sigma}^T\,\hat{\boldsymbol{B}}_m^T. \tag{66}$$

For the elastic fiber:

$$\boldsymbol{L}_f = \boldsymbol{L}_{fe}. \tag{67}$$

The overall stiffness now follows from equation (48), providing that $\boldsymbol{A}_m$ or $\boldsymbol{A}_f$ are known.

As an example we again use the particularly simple results indicated by the Voigt model:

$$\boldsymbol{L} = c_f\,\boldsymbol{L}_f + c_m\,\boldsymbol{L}_m \tag{52}$$

with

$$\boldsymbol{B}_m = \boldsymbol{L}_m\,\boldsymbol{L}^{-1}. \tag{54}$$

Now, $\boldsymbol{L}_m$ from (52) is substituted for the left-hand side in (66), and also into (54). This last result, with (65), is substituted into the right-hand side of (66). Note that $\boldsymbol{L}_m$, $\boldsymbol{L}$, and $\hat{\boldsymbol{Q}}$ are symmetric. After rearrangement, (66) leads to an

implicit expression for $\boldsymbol{L}$:

$$\boldsymbol{L} = \boldsymbol{L}_e - \frac{G_m}{c_m \tau_0^2} \hat{\boldsymbol{Q}} [\boldsymbol{I} - c_f \boldsymbol{L}_f \boldsymbol{L}^{-1}] \boldsymbol{\sigma} \boldsymbol{\sigma}^T [\boldsymbol{I} - c_f \boldsymbol{L}^{-1} \boldsymbol{L}_f] \hat{\boldsymbol{Q}}. \tag{68}$$

Evaluation of the overall stiffness $\boldsymbol{L}$ which corresponds to the i-th increment in stress

$$\boldsymbol{\sigma}_i = \boldsymbol{\sigma}_{i-1} + d\boldsymbol{\sigma}_i$$

can be made in a certain number of iterative steps j, using the recurrence formula.

$$\boldsymbol{L}_{(i,j)} = \boldsymbol{L}_e - \frac{G_m}{c_m \tau_0^2} \hat{\boldsymbol{Q}} [\boldsymbol{I} - c_f \boldsymbol{L}_f \boldsymbol{L}_{(i,j-1)}^{-1}] \boldsymbol{\sigma}_i \boldsymbol{\sigma}_i^T [\boldsymbol{I} - c_f \boldsymbol{L}_{(i,j-1)}^{-1} \boldsymbol{L}_f] \hat{\boldsymbol{Q}}. \tag{69}$$

The iteration starts at $\boldsymbol{L}_{(i,0)}$, which is known from the previous step $(i-1)$, and continues for N steps until a selected convergence criterion is satisfied. For example, one can use

$$(\| \boldsymbol{L}_{(i,N+1)} - \boldsymbol{L}_{(i,N)} \|) / \| \boldsymbol{L}_{(i,N)} \| \leqslant \varepsilon \tag{70}$$

where ε is a suitable error bound, e.g., 10^{-3}, and $\| \ \|$ denotes norm of a matrix.

The updated value of $\boldsymbol{L}$ can now be used to find $\boldsymbol{B}_m$ in (54) and then $d\boldsymbol{\alpha}$ in (59). In this way the Voigt model can be used to identify approximate limits on the extent of the matrix-dominated deformation mode. One can also obtain plastic and total strains in the fiber-dominated mode from the Voigt model, but in view of the assumption involved, such results should be regarded with caution.

4. Selected Results

We can now identify the boundary in stress space between the fiber and matrix-dominated deformation modes of the composite ply. This is best done by comparison of the overall yield surfaces found for the two modes. We recall that the yield surface in the matrix-dominated mode, given by equations (16)–(18) is a straight cylinder with the cross section in Fig. 2, and with generators parallel to the σ_{11} stress axis. The shape of this yield surface does not depend in any way on fiber or matrix elastic properties, but, of course, the magnitude of the ply yield stress τ_0 may be affected by the fiber volume fraction. Furthermore, if the ply does not harden, the matrix-dominated yield surface remains fixed during deformation. In contrast, the fiber-dominated yield surface is affected by fiber and matrix elastic properties and by phase volume fractions. This dependence is introduced through the elastic stress concentration factor $\boldsymbol{B}_{me}$, which depends on phase properties as indicated, for example, by (54). Of course, this surface also translates during fiber-dominated plastic deformation, c.f., equation (59).

Accordingly, the comparison of the two modes is best done in terms of initial yield surfaces of the ply. This is shown in the sequel for two fibrous composite systems, boron-aluminum and graphite-aluminum. Phase properties are given

Table 1. *Elastic Properties of Selected Matrix and Fiber Materials*

	E_A (10^6 psi) [GPa]	G_A (10^6 psi) [GPa]	ν_A	E_T (10^6 psi) [GPa]	G_T (10^6 psi) [GPa]
6061 Aluminum	10.5 [72.5]	3.95 [27.2]	0.33	10.5 [72.5]	3.95 [27.2]
Boron	58.0 [400.0]	24.2 [166.8]	0.20	58.0 [400.0]	24.2 [166.8]
T-50 Graphite	56.0 [386.4]	2.2 [15.2]	0.41	1.1 [7.6]	0.38 [2.6]

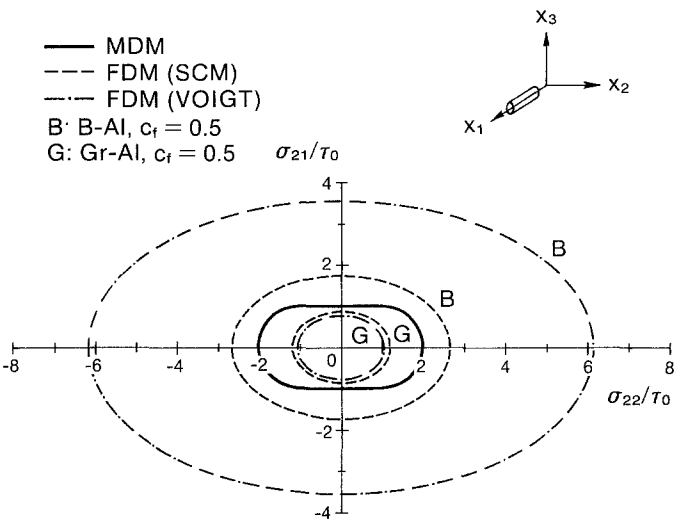

Fig. 4. Initial yield surfaces in the $\sigma_{21}\sigma_{22}$-plane. Comparison of fiber-dominated (FDM) and matrix-dominated (MDM) yield modes in boron and graphite-aluminum composite systems

in Table 1, the phase volume fractions were selected as $c_f = 0.5$ for both systems. To facilitate labeling of the yield surfaces we use the following abbreviations:

MDM – yield surface for the matrix-dominated deformation mode
FDM – yield surface for the fiber-dominated deformation mode
SCM – yield surface for the self-consistent model of the composite
VOIGT – yield surface for the Voigt model of the composite
B – yield surface of the B-Al ply
G – yield surface of the Gr-Al ply.

Figure 4 shows the various yield surfaces of Figs. 2 and 3 in the $\sigma_{22}\sigma_{21}$-plane.

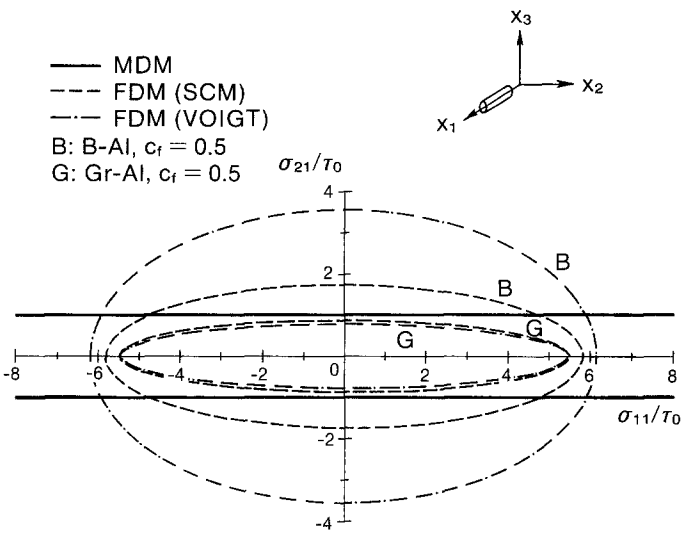

Fig. 5. Initial yield surfaces in the $\sigma_{21}\sigma_{11}$-plane. Comparison of fiber-dominated (FDM) and matrix-dominated (MDM) yield modes in boron and graphite-aluminum composite systems

For the boron-aluminum system the yield surfaces of the fiber-dominated mode are generally larger than the yield surface of the matrix-dominated mode, hence plastic deformation in the $\sigma_{22}\sigma_{21}$-plane starts, for most loading directions, in the matrix mode. The opposite is true for the graphite-aluminum system. There, the FDM yield surfaces always lie within the MDM surface. Also, the Voigt and SCM surfaces are almost identical.

The longitudinal sections of the yield surfaces, in the $\sigma_{11}\sigma_{21}$-plane are indicated in Fig. 5. The earlier comments again apply. The fiber-dominated mode now affects plastic deformation of the B-A*l* system at high ratios of σ_{11}/σ_{21}, the FDM yield surface forms end caps of the overall surface which is primarily matrix-dominated. Response of the Gr-A*l* system is dominated by the fiber mode. During plastic loading the FDM yield surface will translate according to equation (59).

Figure 6 shows what may be regarded as a top view of the yield surfaces in the $\sigma_{11}\sigma_{22}$-plane. It makes it apparent that the B-A*l* system deforms in matrix-dominated mode in most instances, except when the axial normal stress σ_{11} in the fiber direction x_1 is very high in comparison to other stress components. Also, it is now clear that the initial yield surfaces for the graphite-aluminum ply are always of the fiber-dominated mode, and that both the self-consistent and Voigt approximations give very similar shapes.

The differences in shape and size of yield surfaces of the boron-aluminum and graphite-aluminum systems are caused by the different longitudinal shear moduli G^f_A of the fiber. This is suggested by Table 1, and it can be verified

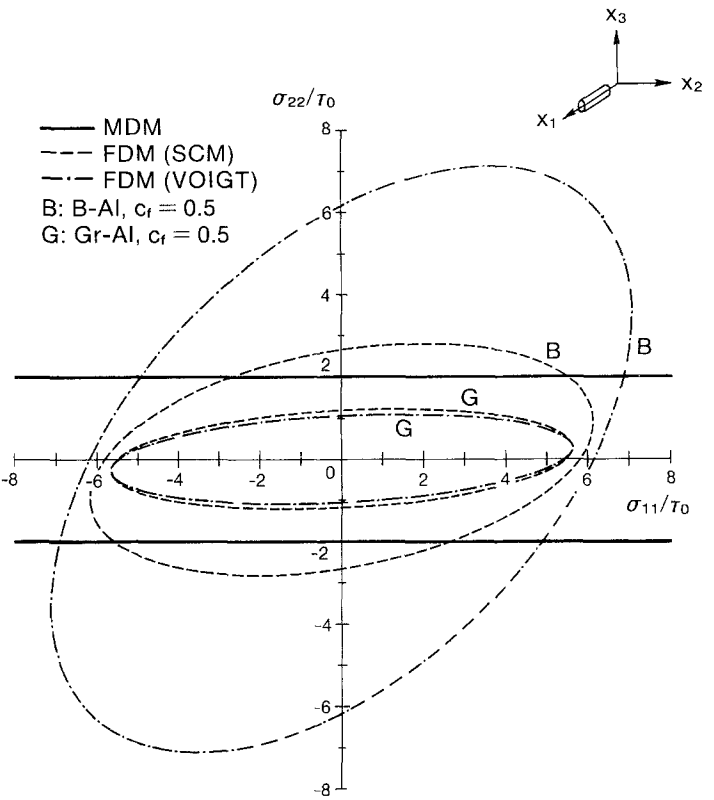

Fig. 6. Initial yield surfaces in the $\sigma_{22}\sigma_{11}$-plane. Comparison of fiber-dominated (FDM) and matrix-dominated (MDM) yield modes in boron and graphite-aluminum composite systems

analytically. The implication is that fibers with a large shear rigidity prevent plastic slip on planes which intersect the fiber axis, while more compliant fibers cannot serve as equally effective barriers to slip.

5. Comparison with Experiments

In a related program, conducted, in part, at Yale University by the late Professor Aris Phillips, and by his students Dr. Y. Macheret and Mr. C. H. Liu, initial yield surfaces were found for an annealed 6061 Al-B ply in several stress planes. These experiments were performed on tubular specimens reinforced in the axial direction by aligned boron fibers. The tubes were 38 mm in diameter, about 200 mm long, and the wall thickness was 1.27 mm, i.e., about seven monolayers of fiber; $c_f = 0.45$. The onset of yielding of the tubes was determined in incremental tension, torsion, and internal pressure, following the method described by Phillips et al. [7] and using the definition of yielding in terms of proportional limit with zero offset.

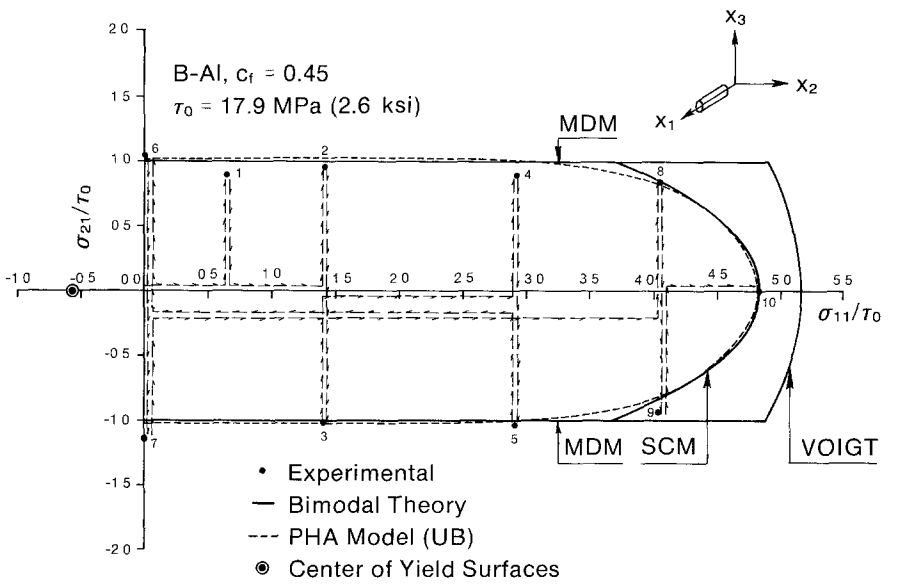

Fig. 7. Initial yield surfaces of a B-Al composite in the $\sigma_{21}\sigma_{11}$-plane. Comparison of experimental results with yield surfaces derived from the bimodal plasticity theory and from the periodic hexagonal array (PHA) model

Figure 7 shows results for combined torsion and axial tension, with loading paths and individual yield points numbered according to the loading sequence. The yield surfaces which appear in the figure were calculated as those in Fig. 5, with τ_0 selected for best fit of the data. The center of the surface was found from an interpolation of the yield points 8, 9, and 10 by the fiber-dominated branch of the yield surface found from the self-consistent model. The Voigt model yield surface is shown for comparison.

Figure 7 also shows the yield surface found from the periodic hexagonal array (PHA) model of the composite medium [1], [2]. This model provides estimates of upper and lower bounds on overall instantaneous properties and thus permits calculation of stress-strain curves which bracket that of an actual composite along a given loading path. The bounds are rigorous in the initial part of elastic deformation. The PHA model yield surface was obtained from several calculated stress-strain curves, with the same definition of yielding as that used in the experimental evaluation of the yield points.

Figure 8 presents results obtained from continuation of the experiment, now under torsion, internal pressure, and axial compression adjusted so that $\sigma_{11} = 0$. Again, the yield surface, and its center, were obtained by fitting the matrix-dominated branch of the yield surface shown in Fig. 4. Also, the upper and lower bound yield surfaces found with the PHA model are plotted in Fig. 8.

Figure 9 shows the last set of data obtained for the tube which was then

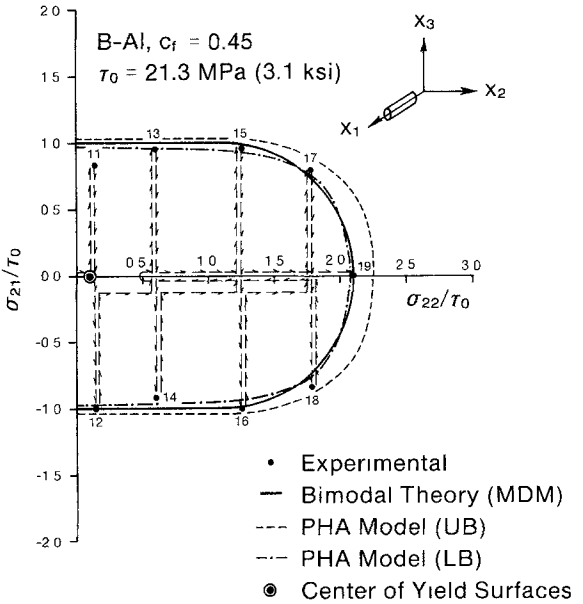

Fig. 8. Initial yield surfaces of a B-Al composite in the $\sigma_{21}\sigma_{22}$-plane. Comparison of experimental results with the yield surface of matrix-dominated mode. and with surfaces derived from the periodic hexagonal array (PHA) model

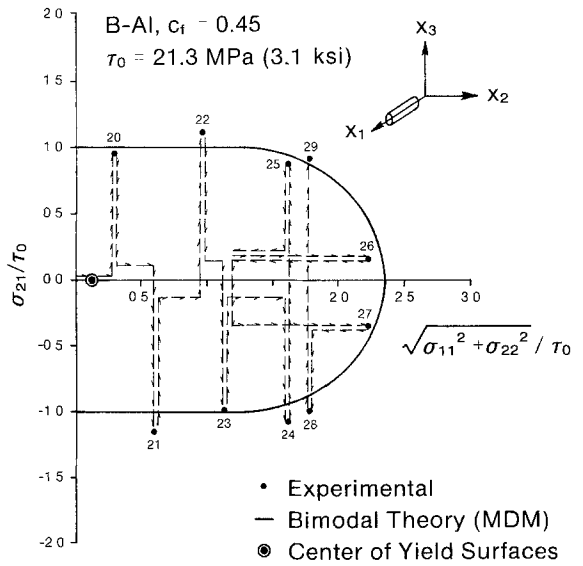

Fig 9 Initial yield surface of a B-Al composite tube under internal pressure and torsion. Comparison of experimental results with the yield surface of the matrix-dominated mode

loaded only by torsion and internal pressure so that the axial stress $\sigma_{11} = \sigma_{22}/2$. The yield surface and its center were constructed as a section of the surface found in Fig. 8 in the current stress plane.

These results agree well with the theoretical predictions. Note, however, that the τ_0 in Fig. 7 is somewhat smaller than that in Figs. 8 and 9. The reasons for the difference are not known; they may be possibly related to strain hardening caused during the few plastic loading steps which are necessary to determine the yield point on each loading path.

It is significant that the experimental points in Figs. 8 and 9 confirm the existence of the matrix-dominated yield surface given by equations (16)–(18). The $f_a(\boldsymbol{\sigma})$ branches appear to be circular and this justifies the assumption, made in equation (7), that the ply yield stress τ_0 is independent of the slip direction. Further support for the bimodal plasticity theory is provided by its agreement with the predictions given by the PHA model. We note that a very good agreement also has been found between the PHA and the SCM or Voigt yield surfaces for the graphite-aluminum system shown in Figs. 4 to 6. This reinforces one's confidence in the bimodal theory, at least with regard to initial yielding.

6. Discussion

The existence of the two deformation modes was recognized in some of the early investigations of inelastic behavior and failure of metal matrix composites [8]–[10]. A deformation mechanism similar to the matrix-dominated plastic yielding was also identified by Spencer and associates [11]–[13] in plastically incompressible, rigid-perfectly plastic materials reinforced by inextensible fibers. It is probably obvious that fiber inextensibility is sufficient but not necessary for slip to take place only on planes parallel to the fiber axis. Indeed, Helfinstine and Lance [14], in their study of such ideal fiber reinforced materials of the Tresca type, found a yield surface of the same shape as that shown in Fig. 2.

In the present work the matrix-dominated mode was obtained from entirely different assumptions. Plastic incompressibility was recovered from these assumptions, but elastic response of both the fibers and the composite were preserved. This is an advantage in many applications where the elastic and plastic strains are of comparable magnitude. Also, it was found that the presence of the matrix-dominated mode in a particular composite system depends on the fiber shear stiffness G_A^f, rather than on the axial Young's modulus E_A^f which is related to extensibility of the fibers. For example, Figs. 5 and 6 show that very different deformation modes exist in the Gr/Al and B/Al systems, even though the fibers have similar axial Young's moduli.

Clearly, neither the self-consistent method, nor the Voigt model are able to detect the matrix-dominated mode, but they appear to predict initial yield surfaces of the fiber-dominated mode which are in agreement with experiments, and also, as we found herein and in a related but as yet unpublished study on

the graphite-aluminum system, with the bounds obtained from the periodic hexagonal array model. At least for the Gr/Al system, the limitations of the self-consistent method appear to be less severe than previously thought [15].

Although we did not present here comparisons between the experiments and the predictions obtained from our Vanishing Fiber Diameter (VFD) model [16]. we would like to point out that for the plane stress case considered the model predicts an ellipsoidal yield surface with axes σ_{11}, σ_{22}, σ_{21}, which is contained within the MDM/FDM envelope, and which has points of contact with this envelope at all three stress axes. Therefore, the VFD model tends to underestimate the onset of yielding, and it also suggests plastic strain directions which are different from those indicated by the present results.

In many respects the present work reconciles the various plasticity theories of fibrous composites and suggests limits of their validity; but, additional comparisons are needed with experiments in the hardening range, to establish such connections and limitations as may exist in a broader spectrum of material response.

Practical applications of the present results are anticipated in problems where extensive matrix-dominated plastic straining is evident. For example, this appears to be the case in unidirectional plies and laminates which are reinforced by fibers of high shear rigidity and contain cracks or similar stress concentrations.

Acknowledgements

This work was supported, in part, by the Office of Naval Research, and by the Army Research Office. The authors are indebted to Mr. Rick Hall and Mr Rahul Shah for numerical evaluation of the initial yield surfaces, and to Dr. Y. Macheret and Mr. C. H. Liu for their experimental data.

References

[1] Dvorak G. J., Teply, J. L., Periodic hexagonal array models for plasticity analysis of composite materials. In: Plasticity today, modelling, methods and applications. W. Olszak memorial volume (Sawczuk, A., Bianchi, V. eds.) p 623 Elsevier 1985.

[2] Teply, J. L., Dvorak, G. J.: Bounds on overall instantaneous properties of elastic-plastic composites. To appear in the Journal of the Mechanics and Physics of Solids.

[3] Hill, R.: Elastic properties of reinforced solids some theoretical principles. J. Mech Phys. Solids **11,** 357–372 (1963).

[4] Walpole, L J.: On the overall elastic moduli of composite materials. J Mech. Phys. Solids **17,** 235–251 (1969).

[5] Huang, W C : Plastic behavior of some composite materials J. Composite Materials **5,** 320–338 (1971).

[6] Yamada, Y., Yoshimura, N., Sakurai, T . Plastic stress-strain matrix and its application for the solution of elastic-plastic problems by the finite element method Int. J. Mech. Sci. **10,** 345–354 (1968).

[7] Phillips, A., Liu, C. S., Justusson, J. W.: An experimental investigation of yield surfaces of elevated temperatures Acta Mechanica **14,** 119–146 (1972)

[8] Stowell, E. Z., Liu, T. S. On the mechanical behavior of fiber-reinforced crystalline materials J. Mech. Phys. Solids **9**, 242–260 (1961).
[9] Kelly, A., Davies, G. J.: The principles of fiber reinforcement of metals. Metallurgical Reviews **10**, 1–77 (1965).
[10] Cratchley, D.: Experimental aspects of fiber-reinforced metals. Metallurgical Reviews **10**, 79–144 (1965).
[11] Mulhern, J. F., Rogers, T. G., Spencer, A. J. M.: A continuum model for fiber-reinforced plastic materials. Proc. Roy. Soc. **301**, 473–492 (1967).
[12] Spencer, A. J. M.: Deformation of fibre-reinforced materials. Oxford University Press 1972.
[13] Spencer, A. J. M. (editor). Continuum theory of the mechanics of fibre-reinforced composites. CISM courses and lectures No. 282. Springer 1984.
[14] Helfinstine, J. D., Lance, R. H.: Yielding of fiber reinforced Tresca material. J. Engineering Mechanics Division ASCE, **EM 4**, 849–866 (1972).
[15] Dvorak, G. J., Bahei-El-Din, Y. A.: Elastic-plastic behavior of fibrous composites. J. Mech. Phys. Solids **27**, 51–72 (1979).
[16] Dvorak, G. J., Bahei-El-Din, Y. A : Plasticity analysis of fibrous composites. J. Applied Mechanics **49**, 327–335 (1982).

Prof G J. Dvorak and Dr. Y. A. Bahei-El-Din
Department of Civil Engineering
Rensselaer Polytechnic Institute
Troy, NY 12180
U.S.A.